❑   1767

An efficient inductor-capacitor-inductor-capacitor compensation topology for wireless power transfer system

Talha Irshad, Malik Nauman, Pg Emeroylariffion Abas
Faculty of Integrated Technologies, Universiti Brunei Darussalam, Brunei Muara, Brunei Darussalam

Article Info	**ABSTRACT**
Article history: Received May 23, 2024 Revised Oct 6, 2024 Accepted Nov 28, 2024	Wireless power transfer (WPT) systems provide a promising alternative for charging various applications, including electric vehicles (EVs), biomedical implants, smartphones, and network sensors. However, these systems often struggle to maintain high efficiency under varying loading and coupling conditions. This paper addresses these challenges by proposing a novel hybrid inductor-capacitor-inductor-capacitor (LC-LC) compensation topology. The proposed LC-LC topology is specifically designed to outperform conventional single-element compensation topologies, such as series-series (SS) and series-parallel (SP) configurations, by effectively reducing leakage inductance between coils. An analytical model of the LC-LC topology is developed and validated through simulations using Keysight advanced design system (ADS) software. The results demonstrate that the LC-LC topology not only achieves a peak efficiency of 99.6% under optimal conditions but also maintains superior performance compared to SS and SP topologies, with only a slight decrease to 93% efficiency observed at low load resistances. These findings highlight the potential of the LC-LC topology to significantly enhance WPT system efficiency across a range of operating conditions.
Keywords: Compensation topology Coupling coefficient Magnetic resonance coupling Mutual inductance Power transfer efficiency Resonance frequency Wireless power transfer	

Corresponding Author:

Pg Emeroylariffion Abas
Faculty of Integrated Technologies, Universiti Brunei Darussalam
St. Tungku Link, Gadong, Brunei Muara BE1410, Brunei Darussalam
Email: emeroylariffion.abas@ubd.edu.bn

1.   INTRODUCTION

The wireless power transfer (WPT) system is the wireless transmission of energy that provides a compelling alternative to conventional charging systems [1], [2], finding applications for the charging of electric vehicles (EVs) [3], portable devices, including laptops and smartphones [4], as well as for powering biomedical implants [5]. Near-field electromagnetic induction techniques, such as inductive and magnetic resonance coupling (MRC) [6], significantly impact WPT system design, with MRC offering higher coupling efficiency when tuned to the same resonance frequency [7], [8]. The MRC technique is widely used in WPT systems, particularly for applications requiring minimal power, like charging handheld devices and sensors [9]. In the design process of a WPT system, different components, including coils [10], [11], compensation networks, and power converters (inverters and rectifiers) [4], [12], need to be considered, taking into account their application [4], [10], [12]. The WPT design aims for optimal energy transfer efficiency, load-independent output voltage and current, and a high-quality factor. Among these components of a WPT system, compensation networks play a critical role in maximizing power transfer efficiency (PTE), minimizing leakage inductance (resulting from magnetic field coupling), and capacitance (related to electric field coupling) generated by the coils and capacitor plates, respectively.

Compensation topologies in the WPT system, include single-resonant/single-element and hybrid/multi-element structures, with four fundamental network topologies: series-series (SS), series-parallel (SP), parallel-series, and parallel-parallel [13]-[15]. On the other hand, hybrid compensation topologies employ multiple capacitors and inductors as compensation elements. Extensive research has been conducted on both single and multi-element compensation topologies including a comparative study between single-element SS and SP topologies aimed at optimizing EV charging [16], as well as a study by Zhang *et al.* [17] to determine load-independent voltage transfer ratios and optimal maximum efficiency for single element topologies. Similarly, loss analysis was conducted on a low-power, high-frequency WPT system with SS topology, achieving 2.93 W peak output power and 60% PTE [18]. In terms of the hybrid /multi-element compensation topologies, an LCC-LCL hybrid compensation topology was investigated and compared with double-sided LCL and LCL-LCC topologies for performance optimization [19]. The investigation reveals the proposed LCC-LCL topology achieved 94% efficiency with an output power of 111 W as compared to 90% and 88% efficiency with 104W and 99W output power for DS-LCL and LCL-LCC topologies, respectively. An LC-S compensated WPT system with a 2 W output power and 84.4% efficiency was developed for implantable pacemaker charging [20].

The air gap between the transmitting and receiving coils causes leakage inductance in a simple WPT system without resonance; the leakage increases with the increase in the distance between the coils [21]. To mitigate this leakage, capacitors are often introduced [22]. The resonant tank formed by capacitors and inductors minimizes power leakage by ensuring the transmitter and receiver resonate at the same frequency, thereby improving PTE and minimizing current flow [23]. Achieving high PTE remains a key goal, regardless of load resistance and coupling coefficient variations. Series-compensated SS and SP topologies frequently struggle to achieve high performance, particularly under changing load and coupling conditions. Analysis of the SS and SP compensation topologies reveals that the variations in loading and coupling conditions, as well as changes in frequency, quality factor, and coil design, all have an impact on PTE. As a result, this paper proposes a hybrid LC-LC compensation topology and compares it to the series-compensated SS and SP compensation topologies. The proposed LC-LC topology provides several advantages, including a high coupling coefficient and load-independent output characteristics. It also offers high PTE across varying load resistances and coupling coefficients. The rest of the paper is organized as: section 2 describes the proposed LC-LC compensation topology, including the circuit model and design analysis. Section 3 presents the simulation results and compares the proposed topology to other compensation topologies. Finally, section 4 summarizes the work and proposes future research directions in this area.

2. METHOD

This paper proposes an LC-LC compensation topology (Figure 1(a)), which consists of a series compensation capacitor with a compensation inductor on both the primary and secondary circuits. The proposed compensation topology was compared to the series compensated SS and SP compensation topologies (Figures 1(b) and (c)). L_1 and L_2 represent the self-inductances of the transmitter and receiver coils, respectively, while C_1 and C_2 represent the transmitter and receiver compensation capacitors. The load resistance is denoted by R_L, the input resistance of the primary side is denoted by Rin, and the input voltage source is denoted by V_s. L_P and L_S are the additional compensation inductors added to the primary and secondary sides, respectively. Figure 2 represents the schematic diagram for the transmitter and receiver's coil dimensions, such as transmission distance d, the radius of wire R_i, the radius of coil r_i, and the number of turns N_i.

(a)

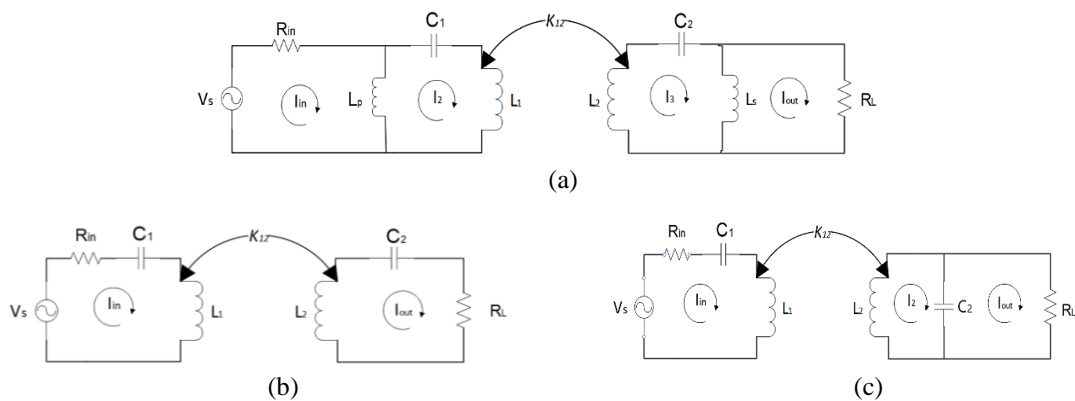(b)   (c)

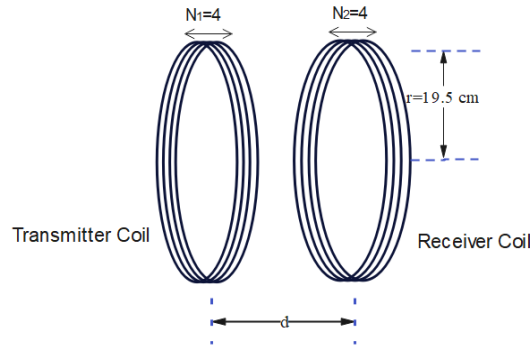Figure 1. Schematic diagrams for the; (a) LC-LC, (b) SS, and (c) SP topologies

Figure 2. Schematic diagram representing the coil's structure

Self-inductance L_i of coil i ($i=1, 2$) is determined by the number of turns N_i, the radius of the wire R_i and the radius r_i of the coil i [7].

$$L_i = N_i^2 \mu_o \mu_r r_i \left[ln\left(\frac{8r_i}{R_i}\right) - 2 \right], \forall i = 1,2 \tag{1}$$

where, μ_o and μ_r are the freespace permeability and relative permeability, respectively. Mutual inductance M_{12} between the transmitter and receiver coils can then be determined using the Neumann formula for circular coils with a gap distance of d between the transmitter and receiver coils and an angle θ between the coils' axis [24],

$$M_{12} = \frac{2\mu_o N_1 N_2 \sqrt{a+b}}{b} \left[\left(1 - \frac{\beta^2}{2}\right) K(\beta) - E(\beta) \right] \tag{2}$$

where

$$a = \frac{(r_1)^2 + (r_2)^2 + d^2}{(r_1)^2 (r_2)^2}; \ b = \frac{2}{(r_1)(r_2)}; \ \beta = \sqrt{\frac{2b}{a+b}}$$

$$K(\beta) = \int_0^{\pi/2} \left(\frac{d\theta}{\sqrt{1-\beta^2 \sin^2 \theta}}\right); \ E(\beta) = \int_0^{\pi/2} \left(\sqrt{1 - \beta^2 \sin^2 \theta} \ d\theta\right)$$

The rate at which the two inductive coils are magnetically coupled with each other is represented by the coupling coefficient k_{12} between the transmitter and receiver coils. A high coupling coefficient generally results in a higher PTE, and vice versa. The coupling coefficient k_{12} is defined as the mutual inductance divided by the product of the self-inductance of two coils [25].

$$k_{12} = \frac{M_{12}}{(\sqrt{L_1 L_2})}, 0 < k < 1 \tag{3}$$

For the proposed compensation network in Figure 1(a), the reactance of the circuit and the intended resonance frequency f_o can be used to estimate the values of the compensating capacitors, C_1 and C_2,

$$C_1 = \frac{1}{(2\pi f_o)^2} \left(\frac{1}{L_P + L_1}\right); \ C_2 = \frac{1}{(2\pi f_o)^2} \left(\frac{1}{L_S + L_2}\right) \tag{4}$$

Kirchhoff's voltage law can be utilized on the transmitter and receiver circuits of the proposed compensation network, to establish expressions for power delivered (P_{in}) and power dissipated (P_{out}). Finally, the WPT efficiency (η_{LC-LC}) from source to load can be calculated using P_{in} and P_{out}.

$$\eta_{LC-LC} = \frac{P_{out}}{P_{in}} = \frac{R_L |I_{out}|^2}{|V_s I_{in}|} \tag{5}$$

Given that P_{in} and P_{out} by the load can be derived as (6) and (7):

$$P_{in} = |V_s I_{in}| = \left[(R_{in} + \omega L_p)|I_{in}| - \omega L_p |I_2| \right] |I_{in}| \tag{6}$$

$$P_{\text{out}} = \frac{\left(\omega^3 k_{12} L_p L_s |I_{in}|\right)^2 L_1 L_2 R_L}{\left[(\omega L_s + R_L)\left\{\left(\omega L_s + \omega L_2 - \frac{1}{\omega C_2}\right)\left(\omega L_p + \omega L_1 - \frac{1}{\omega C_1}\right) - (\omega k_{12})^2 L_1 L_2\right\} - (\omega L_s)^2 \left(\omega L_p + \omega L_1 - \frac{1}{\omega C_1}\right)\right]^2} \tag{7}$$

PTE (η_{LC-LC}) for the proposed compensation topology can be expressed as (8):

$$\eta_{\text{LC-LC}} = \frac{\left(\omega^3 k_{12} L_p L_s\right)^2 L_1 L_2 R_L |I_{in}|}{\frac{[(R_{in} + \omega L_p)|I_{in}| - \omega L_p |I_2|]}{\left[\left[(\omega L_s + R_L)\left\{\left(\omega L_s + \omega L_2 - \frac{1}{\omega C_2}\right)\left(\omega L_p + \omega L_1 - \frac{1}{\omega C_1}\right) - (\omega k_{12})^2 L_1 L_2\right\} - (\omega L_s)^2\left(\omega L_p + \omega L_1 - \frac{1}{\omega C_1}\right)\right]^2\right]}} \tag{8}$$

$\eta_{\text{LC-LC}}$ can be used to analyze the proposed compensation network, and its performance, particular, in comparison to the series compensated SS and SP topologies.

3. RESULTS AND DISCUSSION

The proposed hybrid LC-LC and series compensated SS and SP compensation topologies were modelled and simulated in keysight advanced design system (ADS) software. Table 1 lists the values of the parameters used for the simulation of the circuits, such as the coil's dimensions, input voltage and resistance. Based on these parameters, self-inductance was determined to be $L_1 = L_2 = 18.3~\mu H$. Compensation capacitor values for the SS and SP compensation topologies were determined to be $C_1 = C_2 = 62~nF$. For the proposed hybrid LC-LC compensation topology, primary and secondary compensation capacitor values $C_1 = C_2 = 25~nF$ were taken based on primary and secondary compensation inductor values $L_P = L_s = 26.5~\mu H$.

Table 1. Important parameters of the circuits used in the simulation

Parameter	Value
Radius r_i of coil i, $\forall i = 1,2$	19.5 cm
Radius of wire R	0.1 cm
Permeability of free space μ_o	$4\pi \times 10^{-7} N/A^2$
Relative permeability μ_r	0.9999
Number of turns N_i of coil i, $\forall i = 1,2$	4
Resonance frequency, f_o	150 kHz
Input resistance R_{in}	1 Ω
Input voltage V_s	21.2 Vrms

Table 2 summarizes the values for the various circuit components stated above. The purpose of the input resistance R_{in} on the primary side is to limit the leakage current and hence reduce the VA rating of the transmitter. At resonance, however, the compensation capacitor with its capacitive reactive power cancels out the combined inductive power produced by the compensation inductor (L_p) together with the self-inductance of coil 1 (L_1).

Table 2. Summary of the derived components values of different topologies

Parameters	Single-element network topologies		Proposed topology
	SS	SP	
Self-inductance $L_1 = L_2$		18.3 μH	
Compensation inductor L_P	N/A		26.5 μH
Compensation inductor L_s	N/A		26.5 μH
Compensation capacitor C_1	62 nF		25 nF
Compensation capacitor C_2	62 nF		25 nF

3.1. Power characteristics of compensation topologies

Figures 3(a)-(f) demonstrates the relationship between input/output power ($P_{\text{in}}/P_{\text{out}}$) and coupling coefficient (k_{12}) for the proposed LC-LC, SS, and SP compensation topologies, with LC-LC topology showing unique patterns with both input and output power exhibiting similar trends, as can be seen in Figures 3(a) and (b). Input and output power generally increases with k_{12}, however, as R_L increases, the power curve peaks and subsequently declines with increasing k_{12}. For both the SS and SP topologies, input power trends downward with k_{12}. Specifically, SS exhibits a trend where higher R_L values are associated with higher input power, however, the converse is observed with SP, where lower R_L values lead to higher input power (Figures 3(c) and (e)). P_{out} for the SS topology initially rises before peaking and subsequently, declines with

an increase in k_{12}; with the power curve reaching its peak earlier at lower R_L (Figure 3(d)). In contrast, the P_{out} generally declines in SP topology with k_{12}, yet it increases initially at low R_L before peaking (Figure 3(f)). Additionally, the P_{out} for the SS and SP topologies is significantly lower than the P_{in}, signifying lower efficiency. The LC-LC topology shows lower input and output power than SS and SP topologies, indicating distinct performance and efficiency dynamics in response to coupling coefficient and load resistance variations.
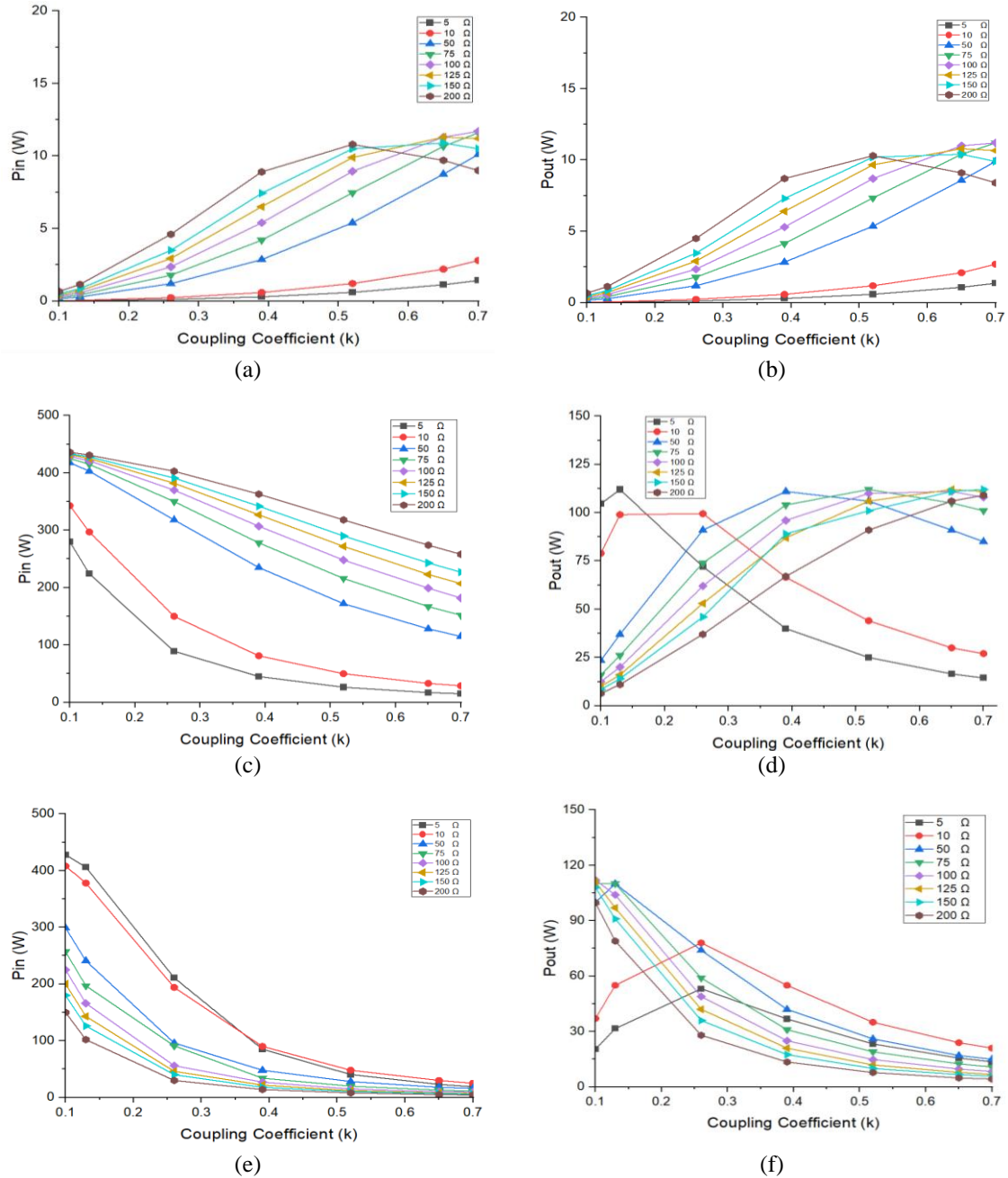
Figure 3. Input/output power for different compensation topologies: (a) input power LC-LC, (b) output power LC-LC, (c) input power SS, (d) output power SS, (e) input power SP topologies, and (f) output power SP topologies

3.2. Current characteristics of compensation topologies

Figure 4 shows the relationship between input/output current (I_{in}/I_{out}) and coupling coefficient (k_{12}) across varying load resistance (R_L) for the proposed LC-LC, SS, and SP compensation topologies. Both the input and output currents of the LC-LC generally increase with k_{12}, as can be seen in Figures 4(a) and (b); with

the input current curve peaking, particularly across large R_L. Whilst large R_L values are associated with high input current, the converse is true for output current, where small R_L generally results in higher output current. I_{out} of SS does not vary much and remains constant with varying k_{12} values (Figure 4(d)), except small R_L values where I_{out} initially increases before peaking and subsequent decline is observed. However, the I_{out} for SP generally decreases with k_{12} (Figure 4(f)). However, I_{out} initially increases across small R_L values, for SP before peaking, followed by a subsequent decline as k_{12} increases. The I_{in} of both SS and SP topologies exhibits a declining trend with k_{12} (Figures 4(c) and (e)). Specifically, large R_L values are associated with higher input current in SS topology, whilst small R_L values are associated with higher input current in SP topology.
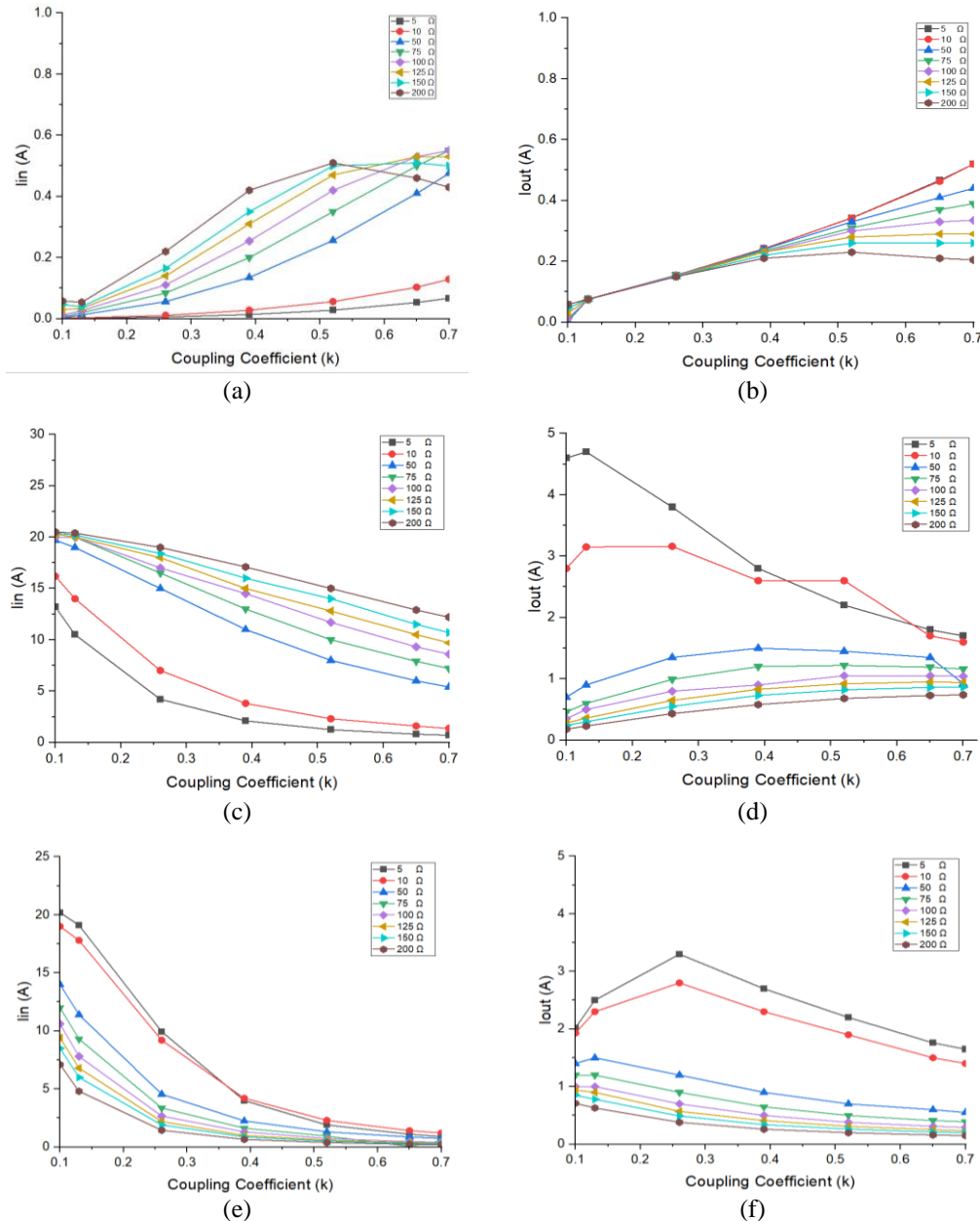

Figure 4. Input/output current for different compensation topologies: (a) input current LC-LC, (b) output current LC-LC, (c) input current SS, (d) output current SS, (e) input current SP topologies, and (f) output current SP topologies

3.3. Voltage characteristics of compensation topologies

Figure 5 shows the relationship between the output voltage (V_{out}) and coupling coefficient (k_{12}) across varying load resistance (R_L). V_{out} for both the proposed LC-LC and SS topologies generally increases with k_{12}

(Figures 5(a) and (b)), with large R_L associated with higher output voltage. An exception to this trend is in the case of small R_L for SS, whereby a slight decreasing trend in V_{out} is observed with k_{12}. This contrasts with the V_{out} trend of SP, with output voltage generally decreasing with k_{12}, as shown in Figure 5(c), except across small load resistance, where a slight peak is observed despite output voltage remaining at approximately the same value. Large load resistance values are associated with a higher output voltage for all three topologies.
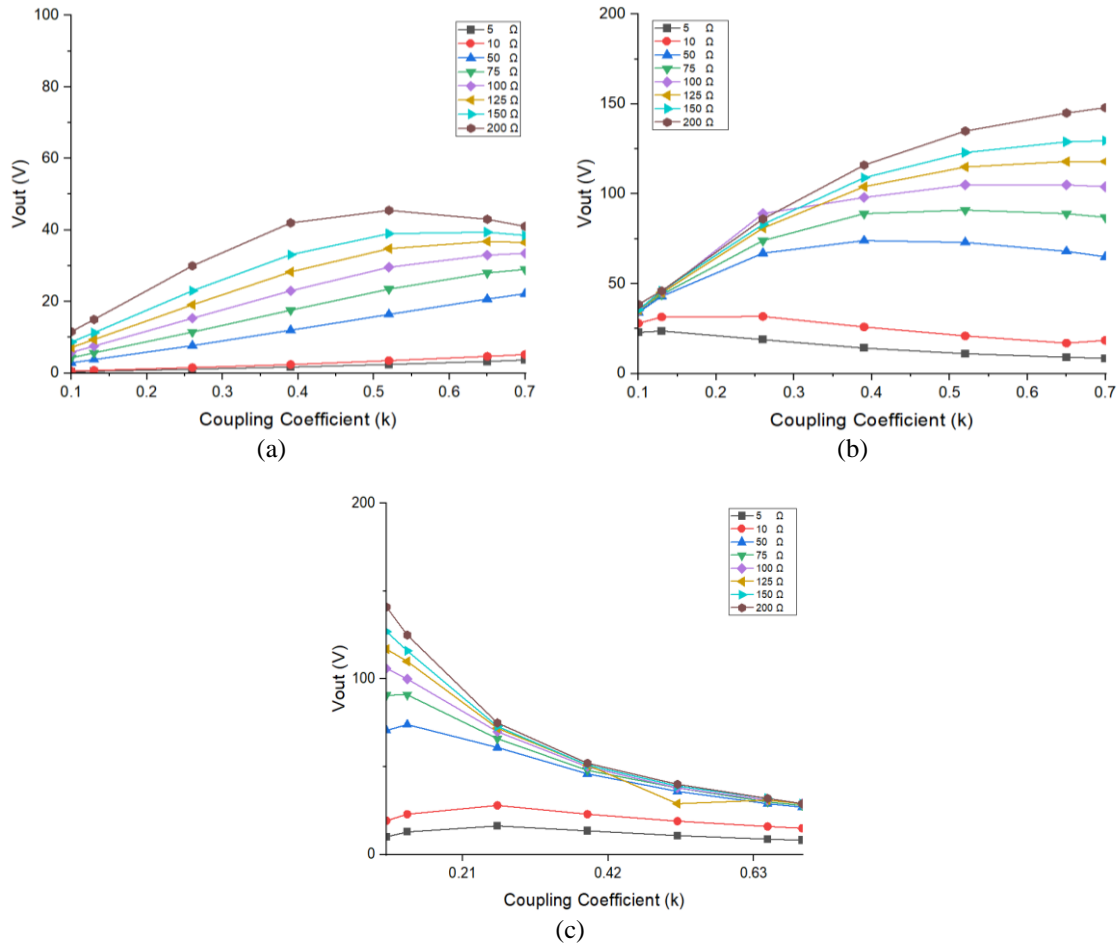

Figure 5. Output voltage for; (a) LC-LC, (b) SS, and (c) SP topologies

3.4. Power transfer efficiency analysis

Figure 6 shows the relationship between the PTE and coupling coefficient (k_{12}) across varying load resistance (R_L). The proposed LC-LC topology in Figure 6(a) shows only a slight decrease in efficiency, particularly across large load resistance values, yet maintains high efficiency across most R_L ranges. Notably, with a coupling coefficient of $k_{12} \leq 0.39$, the efficiency of the proposed LC-LC topology is above 99%, irrespective of the load resistance values. Across a relatively large load resistance value of $R_L = 200$ Ω, efficiency reduces to 93% as the coupling coefficient increases. A peak efficiency of 99.6% is achievable with LC-LC across $R_L = 80$ Ω and $K_{12} = 0.1$. On the other hand, both the SS and SP topologies exhibit increased efficiency with a higher coupling coefficient (Figures 6(b) and (c)), achieving maximum efficiencies of 97% and 98% at specific conditions only; for SS and SP with $k_{12} = 0.7$, across $R_L = 5$ Ω, and $R_L = 200$ Ω, respectively, with performance reducing considerably especially at lower coupling coefficients. Efficiency trends vary across load resistance, with higher efficiency at lower R_L values for SS and higher R_L values for SP, while LC-LC efficiency remains stable, reaching 99.6%. Notably, the lowest efficiency of 93% for the LC-LC topology at $R_L = 200$ Ω and $K_{12} = 0.7$ represents a modest reduction from its peak. The LC-LC topology exhibits superior efficiency, due to its simplified circuit design, which minimizes losses, excluding inverter and rectifier losses.
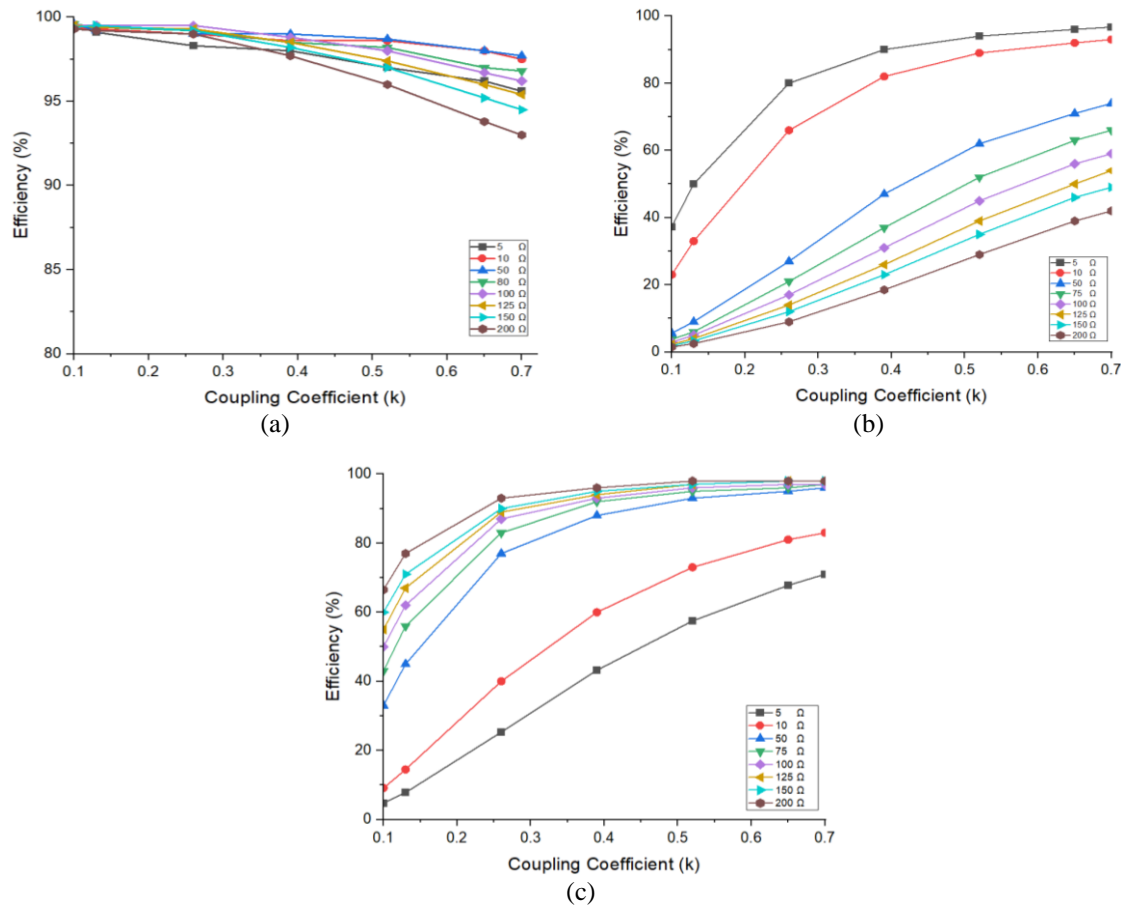
Figure 6. PTE for; (a) LC-LC, (b) SS, and (c) SP topologies

3.5. Frequency response analysis

Figure 7 depicts the relationship between efficiency and frequency for the proposed LC-LC compensation topology at various load resistances. The LC-LC topology exhibits the frequency splitting phenomenon at large load resistance values ($R_L=100 \, \Omega$, $R_L=200 \, \Omega$ (Figures 7(a) and (b)), especially when the coupling coefficient (k_{12}) is increased. At $k_{12}=0.7$, the resonance frequency splits into two halves, with low and high-frequency peaks at 132 and 180 kHz, respectively, for $R_L=200 \, \Omega$ (Figure 7(a)). It is obvious from the Figure 7(b) that the frequency splitting decreases as load resistance decreases. For instance, at $R_L=100 \, \Omega$, the efficiency reduction is small compared to the reduction in efficiency at $R_L=200 \, \Omega$. In Figure 7(b), the frequency curve splits into two halves at $k_{12}=0.7$, with low and high-frequency peaks at 135 kHz and 175 kHz, respectively. The frequency splitting in the proposed LC-LC topology is not observed at small load resistances (Figures 7(c) and (d)), indicating that the resonance frequency is independent of the coupling coefficient. The frequency splitting partly explains the observed reduction in PTE at large load resistance values as the coupling coefficient is increased in Figure 6.

The analysis highlights that the LC-LC topology exhibits load-independent output current characteristics, particularly at a low coupling coefficient of $k_{12} \leq 0.4$. On the other hand, both the SS and SP topologies exhibit load-independent output voltage characteristics at specific conditions: for SS, load-independent output voltage characteristics are observed at $k_{12} \leq 0.2$ and across $R_L \geq 50 \, \Omega$, whilst for SP, at $k_{12} \geq 0.4$ and across $R_L \geq 50 \, \Omega$. The proposed LC-LC topology is suitable for applications requiring stable current, like LED lighting, due to its consistent luminance requirement [26]. On the other hand, SS and SP topologies are ideal for battery charging due to their load-independent output voltage characteristics, allowing constant voltage, particularly within the specific k_{12} and R_L parameters. The analysis further indicates that both SS and SP topologies have high input current and power, resulting in higher volt-ampere (VA) ratings and leading to a significant power loss in the WPT system, which is evident from the efficiencies of the SS and SP topologies. The proposed LC-LC topology, with more reactive elements, demonstrates higher PTE, thereby minimizing power loss and subsequently enhancing PTE. This makes the LC-LC topology especially valuable in applications sensitive to input power variations. These findings also imply that strongly coupled WPT systems,

i.e., strong coupling coefficient, strictly aligned coils and a short transmitter-to-receiver distance are better suited for the SS and SP compensation topologies. On the other hand, the proposed LC-LC topology performs exceptionally well in both strongly coupled and loosely coupled WPT systems; demonstrating efficiency of above 98% and 93%, in a strongly coupled and weakly coupled WPT system. The proposed topology maintains superior efficiency across different transmission distances, distinguishing it from SS and SP topologies. However, it's less suitable for high power applications, but rather more suitable for medium power applications, including the charging of portable devices such as laptops and smartphones with power requirements ranging from a few to 100 watts.

         Table 3 compares the proposed LC-LC topology with other compensation topologies in the literature, in terms of efficiencies and other relevant parameters, highlighting its competitive performance. Despite a lower output power of only *12 W*, LC-LC is extremely efficient; capable of reaching 99.6% efficiency and the lowest efficiency of 93%, focusing on efficiency over maximum transfer of power. This contrasts with SS and SP topologies with peak output powers of *120 W* and *125 W*, respectively, and other hybrid topologies, such as the LC-S and LCC-LCL topologies, exhibiting peak output powers of *2 W* and *111 W* with input voltages of *4.9 V* and *42 V*, respectively. The higher output power of the series compensated SS and SP topologies is attributed to their higher VA rating at the expense of efficiency. In addition, the proposed LC-LC hybrid topology, designed for low power applications, outperforms single element and hybrid compensation topologies in terms of efficiency, despite its low output power.
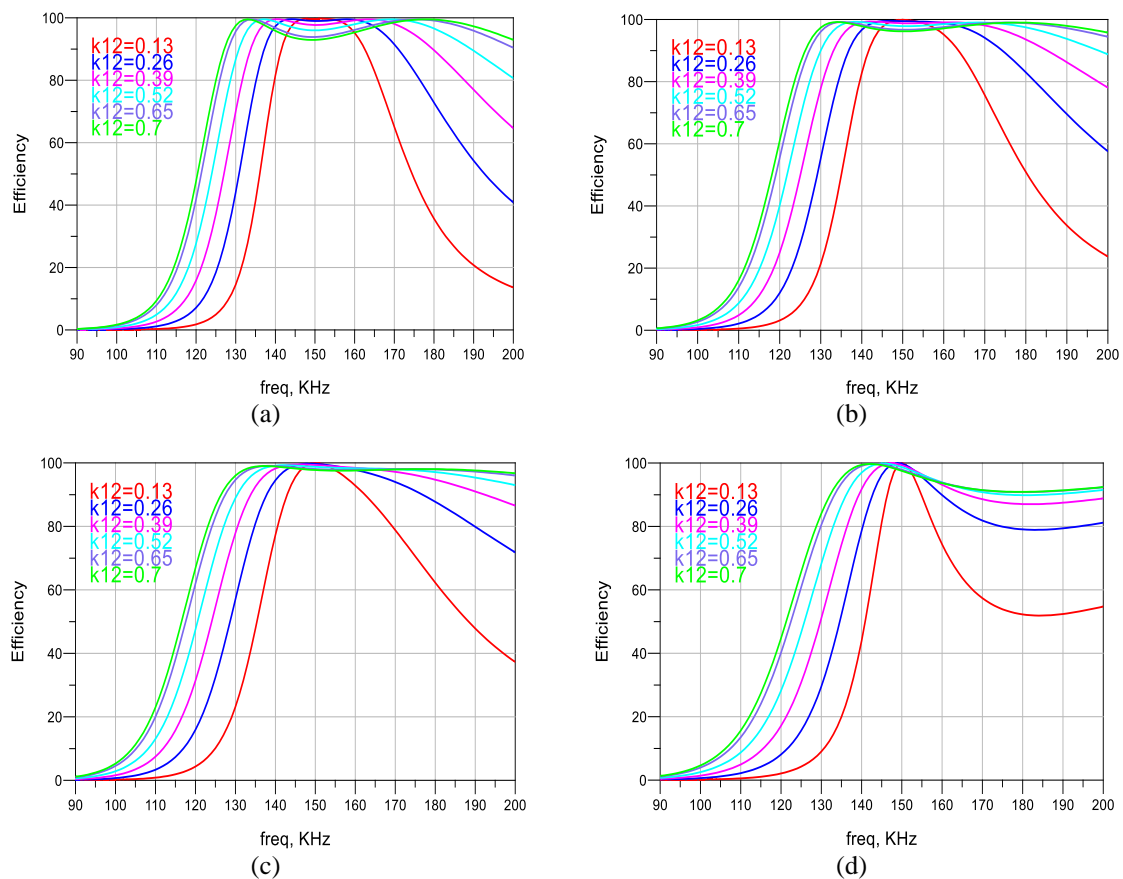

Figure 7. PTE vs frequency for; (a) $R_L=200\ \Omega$, (b) $R_L=100\ \Omega$, (c) $R_L=50\ \Omega$, and (d) $R_L=10\ \Omega$

Table 3. PTE and corresponding parameters of the different compensation topologies

Parameters	LC-LC	SS	SP	LC-S [20]	LCC-LCL [19]
Peak power transfer eff. (%)	99.6	97	98	82.4	94
K_{12} at peak efficiency	0.1	0.7	0.7	N/A	0.2
R_L at peak efficiency (Ω)	75	5	200		N/A
Lowest power transfer eff. (%)	93	2	6		N/A
Var. in eff. from peak eff. (%)	-7	-95	-92		N/A
Input voltage V_{in} (V)		21.2		4.9	42
Resonance frequency (KHz)		150		300	N/A
Output power P_{out}	12 W	120 W	125 W	2 W	111 W

4.   CONCLUSION

WPT faces efficiency challenges as the coupling coefficient fluctuates due to misalignment and changes in the transmitter-receiver distance during charging. Additionally, varying loading conditions can impact PTE and the stability of output current and voltage. To address these issues, a hybrid LC-LC compensation topology is introduced, which outperforms the series compensated SS and SP topologies. The LC-LC topology demonstrated superior PTE across a wide range of loading and coupling conditions, reaching 99.6% and consistently exceeding 95% efficiency. Frequency splitting led to a slight reduction in efficiency to 93% under large load resistance. In contrast, the SS and SP topologies achieved only 97% and 98% efficiency, respectively, with their performance dropping below 10% under significant load variations. These findings highlight the adaptability of the LC-LC topology in both strongly and loosely coupled WPT systems, demonstrating its effectiveness across a wide range of loading and coupling conditions. This study contributes to advancing WPT system performance, with future work including the design and analysis of various hybrid compensation topologies and comparative studies among them. Further research will also focus on optimizing these topologies for high-power applications and integrating dynamic tuning control strategies. Additionally, future studies will explore the development of compact WPT systems and multi-frequency, multi-load systems, which could enhance performance and applicability. Experimental validation and real-world testing of the fabricated design will be crucial to ensure its practical effectiveness and support widespread adoption in WPT applications.

ACKNOWLEDGMENTS

The authors confirm that no personal assistance was provided by individuals outside the scope of authorship for this work. As such, no acknowledgments are necessary.

AUTHOR CONTRIBUTIONS STATEMENT

This journal uses the Contributor Roles Taxonomy (CRediT) to recognize individual author contributions, reduce authorship disputes, and facilitate collaboration.

Name of Author	C	M	So	Va	Fo	I	R	D	O	E	Vi	Su	P	Fu
Talha Irshad	✓	✓	✓	✓	✓	✓	✓	✓	✓	✓	✓		✓	
Malik Nauman					✓	✓				✓	✓	✓	✓	
Pg Emeroylariffion Abas	✓	✓			✓			✓		✓	✓	✓	✓	✓

C : **C**onceptualization	I : **I**nvestigation	Vi : **Vi**sualization
M : **M**ethodology	R : **R**esources	Su : **Su**pervision
So : **So**ftware	D : **D**ata Curation	P : **P**roject administration
Va : **Va**lidation	O : Writing - **O**riginal Draft	Fu : **Fu**nding acquisition
Fo : **Fo**rmal analysis	E : Writing - Review & **E**diting	

CONFLICT OF INTEREST STATEMENT

The authors state no conflict of interest.

INFORMED CONSENT

The study doesn't involve human participants, and therefore, informed consent is not applicable.

ETHICAL APPROVAL

This study didn't involve any human participants, animals, or sensitive data. As such, ethical approval was not required.

DATA AVAILABILITY

The authors confirm that the data supporting the findings of this study are available within the article [and/or its supplementary materials].

REFERENCES

[1]   A. Mahmood, S. Gharghan, M. Eldosoky, and A. Soliman, "Wireless charging for cardiac pacemakers based on class-D power amplifier and a series–parallel spider-web coil," *International Journal of Circuit Theory and Applications*, vol. 51, no. 1, pp. 1–17, Sep. 2022, doi: 10.1002/cta.3420.

[2]   Z. Zhang, H. Pang, A. Georgiadis, and C. Cecati, "Wireless Power Transfer-An Overview," *IEEE Transactions on Industrial Electronics*, vol. 66, no. 2, pp. 1044–1058, Feb. 2019, doi: 10.1109/TIE.2018.2835378.

[3]   M. Venkatesan *et al.*, "A Review of Compensation Topologies and Control Techniques of Bidirectional Wireless Power Transfer Systems for Electric Vehicle Applications," *Energies (Basel)*, vol. 15, no. 20, Oct. 2022, doi: 10.3390/en15207816.

[4]   J. Feng, Q. Li, and F. C. Lee, "Coil and Circuit Design of Omnidirectional Wireless Power Transfer System for Portable Device Application," in *2018 IEEE Energy Conversion Congress and Exposition (ECCE)*, 2018, pp. 914–920, doi: 10.1109/ECCE.2018.8557465.

[5]   C. Kim *et al.*, "Design of miniaturized wireless power receivers for mm-sized implants," *2017 IEEE Custom Integrated Circuits Conference (CICC)*, Austin, TX, USA, 2017, pp. 1-8, doi: 10.1109/CICC.2017.7993703.

[6]   R. Hua and A. P. Hu, "Effect of tuning capacitance of passive power repeaters on power transfer capability of inductive power transfer systems," *Wireless Power Transfer*, vol. 5, no. 2, pp. 97–104, Sep. 2018, doi: 10.1017/wpt.2018.3.

[7]   M. A. Houran, X. Yang, and W. Chen, "Magnetically coupled resonance wpt: Review of compensation topologies, resonator structures with misalignment, and emi diagnostics," *Electronics*, vol. 7, no. 11, pp. 1–45, Nov. 2018, doi: 10.3390/electronics7110296.

[8]   F. Niedermeier, M. Hassler, J. Krammer, and B. Schmuelling, "The effect of rotatory coil misalignment on transfer parameters of inductive power transfer systems," *Wireless Power Transfer*, pp. 77–84, Jun. 2019, doi: 10.1017/wpt.2019.7.

[9]   H. A. Atallah, "Compact and efficient WPT systems using half-ring resonators (HRRs) for powering electronic devices," *Wireless Power Transfer*, vol. 5, no. 2, pp. 105–112, Sep. 2018, doi: 10.1017/wpt.2018.4.

[10] M. A. Houran, X. Yang, W. Chen, and X. Li, "Design and analysis of coaxial cylindrical WPT coils for two-degree-of-freedom applications," *Journal of Physics D: Applied Physics*, vol. 53, no. 49, p. 495004, Oct. 2020, doi: 10.1088/1361-6463/abb33a.

[11] M. A. Houran, X. Yang, and W. Chen, "Two-Degree-of-Freedom WPT System Using Cylindrical-Joint Structure for Applications with Movable Parts," *IEEE Transactions on Circuits and Systems II: Express Briefs*, vol. 68, no. 1, pp. 366–370, Jan. 2021, doi: 10.1109/TCSII.2020.2995616.

[12] P. Darvish, S. Mekhilef, S. Member, H. Azil, B. Illias, and S. Member, "A Novel S-S-LCLCC Compensation for Three-Coil WPT to Improve Misalignment and Energy Efficiency Stiffness of Wireless Charging System," *IEEE Transactions on Power Electronics*, vol. 8993, no. c, Jul. 2020, doi: 10.1109/TPEL.2020.3007832.

[13] B. A. Rayan, U. Subramaniam, and S. Balamurugan, "Wireless Power Transfer in Electric Vehicles: A Review on Compensation Topologies, Coil Structures, and Safety Aspects," *Energies (Basel)*, vol. 16, no. 7, Apr. 2023, doi: 10.3390/en16073084.

[14] K. N. Mude and K. Aditya, "Comprehensive Review and Analysis of Two-element Resonant Compensation Topologies for Wireless Inductive Power Transfer Systems," *Chinese Journal of Electrical Engineering*, vol. 5, no. 2, pp. 14–31, Jun. 2019, doi: 10.23919/CJEE.2019.000008.

[15] A. Agcal, S. O. Ozkilic, and K. Toraman, "Comparison and selection strategy among compensating topologies in two-coil resonant wireless power transfer systems," *Journal of Engineering Research*, vol. 11, no. 2, pp. 148–157, Jun. 2023, doi: 10.36909/jer.14245.

[16] K. Aditya and S. S. Williamson, "Comparative study of Series-Series and Series-Parallel compensation topologies for electric vehicle charging," *2014 IEEE 23rd International Symposium on Industrial Electronics (ISIE)*, pp. 426–430, Jun. 2014, doi: 10.1109/ISIE.2014.6864651.

[17] W. Zhang, S. -C. Wong, C. K. Tse and Q. Chen, "Analysis and Comparison of Secondary Series- and Parallel-Compensated Inductive Power Transfer Systems Operating for Optimal Efficiency and Load-Independent Voltage-Transfer Ratio," in *IEEE Transactions on Power Electronics*, vol. 29, no. 6, pp. 2979-2990, June 2014, doi: 10.1109/TPEL.2013.2273364.

[18] G. Di Capua, N. Femia, G. Petrone, G. Lisi, D. Du, and R. Subramonian, "Power and efficiency analysis of high-frequency Wireless Power Transfer Systems," *International Journal of Electrical Power and Energy Systems*, vol. 84, pp. 124–134, Jan. 2017, doi: 10.1016/j.ijepes.2016.05.005.

[19] J. Jenson, J. P. Therattil, and J. A. Johnson, "A Novel LCC-LCL Compensation WPT System for Better Performance," in 2019 *IEEE International Conference on Electrical, Computer and Communication Technologies (ICECCT), IEEE*, 2019, pp. 1–6, doi: 10.1109/ICECCT.2019.8869513.

[20] S. Cetin and Y. E. Demirci, "High-efficiency LC-S compensated wireless power transfer charging converter for implantable pacemakers," *International Journal of Circuit Theory and Applications*, vol. 50, no. 1, pp. 122–134, Jan. 2022, doi: 10.1002/cta.3150.

[21] S. Li, W. Li, S. Member, J. Deng, and S. Member, "A Double-Sided LCC Compensation Network and Its Tuning Method for Wireless Power Transfer," *IEEE Transactions on Vehicular Technology*, vol. 64, no. 6, pp. 2261–2273, 2015, doi: 10.1109/TVT.2014.2347006.

[22] M. Rehman, P. Nallagownden, and Z. Baharudin, "Efficiency investigation of SS and SP compensation topologies for wireless power transfer," *International Journal of Power Electronics and Drive Systems (IJPEDS)*, vol. 10, no. 4, pp. 2157–2164, Dec. 2019, doi: 10.11591/ijpeds.v10.i4.pp2157-2164.

[23] W. Zhang, S. Member, and C. C. Mi, "Compensation Topologies of High-Power Wireless Power Transfer Systems," *IEEE Transactions on Vehicular Technology*, vol. 65, no. 6, pp. 4768–4778, Jun. 2016, doi: 10.1109/TVT.2015.2454292.

[24] K. Nalty, "Classical calculation for mutual inductance of two coaxial loops in MKS units," *Flux Φ and the Vector Potential A*, pp. 1–8, 2011.

[25] V. Jiwariyavej, T. Imura, and Y. Hori, "Coupling coefficients estimation of wireless power transfer system via magnetic resonance coupling using information from either side of the system," *IEEE Journal of Emerging and Selected Topics in Power Electronics*, vol. 3, no. 1, pp. 191–200, 2015, doi: 10.1109/JESTPE.2014.2332056.

[26] Y. Li, Q. Xu, T. Lin, J. Hu, Z. He, and R. Mai, "Analysis and design of load-independent output current or output voltage of a three-coil wireless power transfer system," *IEEE Transactions on Transportation Electrification*, vol. 4, no. 2, pp. 364–375, 2018, doi: 10.1109/TTE.2018.2808698.

BIOGRAPHIES OF AUTHORS

Talha Irshad received a B.S. degree in electronic engineering from Capital University of Science and Technology, Pakistan, in 2016 and an M.S. in electrical and electronic engineering from Universiti Sains Malaysia, Pulau Pinang, Malaysia, in 2020. Currently, he is a Ph.D. candidate at the Faculty of Integrated Technologies, Universiti Brunei Darussalam. His research interests include wireless power transfer, power electronics, wireless charging, and compensation topologies for wireless power transfer. He can be contacted at email: 21h8452@ubd.edu.bn.

Malik Nauman is an accomplished academic and researcher with over 11 years of experience in Manufacturing, Energy Engineering, and Innovation and Entrepreneurship. He has worked in various universities across the globe, including in Turkey and Saudi Arabia, before joining the Faculty of Integrated Technologies at Universiti Brunei Darussalam as an Associate Professor and Deputy Dean. His research expertise extends beyond energy devices and encompasses other areas, such as image processing and shape memory alloys. He has published numerous research papers and articles in reputed international journals and conferences in these fields. He can be contacted at email: malik.nauman@ubd.edu.bn.

Pg Emeroylariffion Abas received his Bachelor of Engineering in Information System Engineering from Imperial College, London in 2001, before obtaining his Ph.D. in Communication Systems in 2005 at the same institution. After working as an engineer for several years, he joined academia in 2015. He is currently and Senior Assistant Professor in Information System Engineering at the Faculty of Integrated Technologies, Universiti Brunei Darussalam. His present research interests include data analytics, techno-economic analysis, and photonics. He can be contacted at email: emeroylariffion.abas@ubd.edu.bn.